IEEE Access
Multidisciplinary ⋮ Rapid Review ⋮ Open Access Journal

Received 18 May 2023, accepted 4 June 2023, date of publication 8 June 2023, date of current version 21 June 2023.

Digital Object Identifier 10.1109/ACCESS.2023.3284030

RESEARCH ARTICLE

Machine Learning Methods Based on Geophysical Monitoring Data in Low Time Delay Mode for Drilling Optimization

ALEXEY OSIPOV[1], EKATERINA PLESHAKOVA[1,2], ARTEM BYKOV[3], OLEG KUZICHKIN[4], DMITRY SURZHIK[5], STANISLAV SUVOROV[6], AND SERGEY GATAULLIN[1]

[1]Moscow Technical University of Communications and Informatics, 111024 Moscow, Russia
[2]MIREA - Russian Technological University, 119454 Moscow, Russia
[3]Department of Data Analysis and Machine Learning, Financial University under the Government of the Russian Federation, 125167 Moscow, Russia
[4]Department of Informational and Robototechnical Systems, Belgorod National Research University, 308015 Belgorod, Russia
[5]Vladimir State University named after Alexander and Nikolay Stoletovs, 600000 Vladimir, Russia
[6]Department of Applied Informatics, Moscow Polytechnic University, 107023 Moscow, Russia

Corresponding author: Ekaterina Pleshakova (e.s.pleshakova@mtuci.ru)

The work of Dmitry Surzhik was supported by the Intelligent System for Monitoring the Integrity of the Subgrade of the Railway through the Section II "Materials and Methods" under Grant (RFBR) 23-29-10126.

ABSTRACT The purpose of the article is to create an effective method to monitor the state of the drill string and the bit without interfering with the drilling process itself in low-time delay mode. For continuous monitoring of the well drilling process, an experimental setup was developed that operates on the basis of the use of the phase-metric method of control. Any movement of the bit causes a change in the electrical characteristics of the probing signal. To obtain a stable signal from a bit immersion depth of up to 250 m, a frequency of probing electrical signals of 166 Hz and an amplitude of up to 500 V were used; sampling rate (analog-to-digital converter) ADC - 10101 Hz. To identify the state of the drill string and the bit according to the graphs of dependences of changes in the electrical characteristics of the probing signal on time, the authors of the article investigated a number of deep learning methods, based on the results of the research, a line of capsule neural network (CapsNet) methods was selected. The authors have developed two modifications of 1D-CapsNet and Windowed Fourier Transform (WFT) - 2D-CapsNet. To identify the transition between two rock layers with different properties, WFT-2D-CapsNet showed an accuracy of 99%, which is 2-3% higher than the results of modern rock studies based on measurement-while-drilling (MWD) and logging-while-drilling (LWD) methods. The WFT-2D-CapsNet method unambiguously detects self-oscillations in the drill string and detects the good condition of the bit with an accuracy of 99%.

INDEX TERMS Robotics, artificial intelligence, neural networks, engineering, CapsNet, geophysical monitoring, drilling optimization.

I. INTRODUCTION

The problem of providing the population with clean fresh water has long been a key problem of mankind. For areas remote from waterways, drilling artesian wells is a solution to this problem. Aquifers can be at different depths, and to get to them, drilling rigs should be used. This is expensive equipment that is subject to heavy loads and often fails. In 2015-2019, according to statistics, the number of the accidents due to the wear of bits is more than 65% of the total number of all [1] Real-time monitoring of the wear of the bit and timely replacement of bits is important to reduce the frequency of equipment failures. Based on condition-based maintenance (CBM), bit wear can be monitored with real-time condition monitoring signals and wear related. And the quality and efficiency of the design can be significantly improved by replacing the bit to the wear threshold [1].

The associate editor coordinating the review of this manuscript and approving it for publication was Okyay Kaynak.

A. PROBLEMS OF EFFICIENT DRILLING

The problem of drilling efficiency at the transition between two layers of rock with different mechanical properties is discussed in the article by Aribovo et al. [2]. The authors emphasised that the rapid oscillation changes caused by such transitions can damage the bit or significantly affect drilling performance. The authors created a model that allowed them to derive an expression for drilling efficiency for the transition phase. A number of examples given by the authors showed that drilling efficiency is nonlinearly dependent on bit engagement between two rock layers.

The occurrence of self-oscillations in rotary drilling systems leads to a decrease in drilling productivity. The occurrence of self-excited vibrations leads to failure of the bits. The authors of [3] point out that failure of equipment and the increase, in connection with this, the downtime of the drill string range from 2 to 10% of the cost of the well. Because fixed cutter bits (also known as PDC bits) are particularly susceptible to self-exciting vibrations, drilling systems that use these bits. The authors established the relationship between the load on the bit and the stability of the torsion dynamics [4]. Damping of self-oscillations in drill strings with rotating bits is the focus of many studies aimed at revealing the mechanisms of self-excitation [5], [6], [7].

Inspired by this publication, we set ourselves the task of finding methods to prevent damage to the drill string and the bit.

Published studies of sticking and sliding attribute vibrations to static friction effects resulting from the interaction between the rock and the bit [8], [9], [10]. Vibrations caused by bit-to-rock contact cause strong torsional and axial vibrations in the drill string. Sticking oscillations are considered in the study by modeling the drill string as a torsional pendulum, and the interaction between the bit and the rock is considered as Coulomb friction. [11], [12], [13], [14], [15]. Initially, the main attention in the works was paid to longitudinal vibrations of the drilling structure, although later the influence of torsional vibrations of the drill string was considered [16]. Torsional vibrations can cause drill string fatigue and can be strong enough to damage the bit.

The authors of [17] and [18] analyze self-excited axial and torsional vibrations of rotary drilling systems using a model that combines the representation of a drilling structure with several degrees of freedom and a speed-independent law of interaction between the bit and rock. The authors found that axial vibrations propagating along the drill string appear as traveling waves, while torsional vibrations take the form of standing waves, the frequency of which coincides with the torsional resonance of the drill string, excited by the interaction of the bit with the rock. The authors of [19] described an active damping system that significantly reduces the threshold value through the use of feedback control, thus expanding the operating range for vibration-free rotation.

Extending the life of PDC bits without compromising their performance is essential in well drilling. The PDC cutter is the main cutting element of a polycrystalline diamond (PDC) bit [20]. During the drilling process, the PDC cutter is subjected to twisting of the drill cord and rock abrasion under high pressure and strong impact [21], [22]. Changes in the value of cutting forces and torque on the bit lead to torsional vibrations [23], [24] of the drill string. Torsional vibrations lead to the development of longitudinal vibrations. According to the results of the analysis of bit cutters, failures are mainly associated with polycrystalline wear, abrasive wear and cutter failure [25], [26]. The most common wear mechanism for PDC bits in rock drilling is abrasion. Impact resistance is one of the important indicators of the performance and quality of a PDC cutting tooth [27], [28]. Various new designs of PDC bits are created for specific geological conditions, increasing their efficiency and fault tolerance [29], [30].

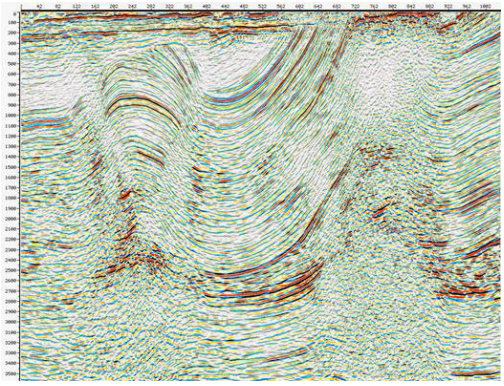

FIGURE 1. Seismic profile.

B. GEOPHYSICAL RESEARCH METHODS

Geophysical methods can be divided into four main groups: potential methods; electrical and electromagnetic (EM) methods, and seismic methods, radiometric methods. Each method has a specific scope, depending on the physical properties and purpose. [31], [32].

Most geophysical methods have been developed for the oil and gas industry. These methods have been developed for various hydrocarbon detection approaches; these methods may not always be transferable from oil and gas to water. Each method has a specific application, depending on the physical properties of the target and how accurately these properties can be detected using available technologies.

Seismic reflection techniques are the most popular methods for mineral exploration and mine planning [31], [33], [34], [35]. Seismic waves generated by a vibrating controlled source are one of the main methods of underground research in geophysics.

Based on records of seismic waves, it is possible to reconstruct subsurface geology in detail. Seismic data can be used to estimate the depth of an aquifer and confirm its presence. These data are also used for design planning.

The traditional method is to transmit electromagnetic pulses with a given fundamental frequency into the surrounding rock. These signals are reflected in places of material

changes, inhomogeneities, or discontinuities. In accordance with the reflection from the inhomogeneity, the signal is returned to the measuring system and recorded and stored digitally for further analysis.

The growing demand for minerals requires the search for new deposits, often at deeper levels, and the improvement of existing methods. The 3D seismic method is widely used in oil exploration [36]. Methods for monitoring elastic wave parameters of geotechnical materials include elastic wave tomography and seismic reflection. Trung et al. proposed a three-dimensional (3D) elastic full-wave inversion tomography method to determine the geotechnical characteristics of a material [37]. Oudphui et al. used 3D seismic data to search for undiscovered mineral deposits [38]. Place et al. improved hard rock image fidelity with a controlled source of seismic noise and identified undeveloped reservoirs and faults [39].

C. ORGANISATION OF CONTROL OF THE DRILLING PROCESS

Vector measuring systems are highly efficient [40], [41], [42] and can be used to detect and locate geodynamic processes. This control method has a high noise immunity and sensitivity compared to fixing the amplitude parameters of the anomalous components of the electromagnetic field. In this case, the object of control is the technological equipment, the well and the surrounding soil.

The papers [43], [44] explain the application of the phase-metric method of geoelectric control, namely the use of several sources of probing signals located in the immediate vicinity of the object under study, and the required number of vector sensors for measuring the electric field. In this case, the registration of phase characteristics at a fixed position of the source and measuring base, with the possibility of controlling the parameters of the probing signals, is based on the fact that the primary and secondary electric fields are vector quantities.

In accordance with the foregoing, it can be concluded that it is possible to organize a drilling process control system in order to prevent processes that lead to damage to the drill string and the bit. At the same time, it is possible to improve the detection accuracy of aquifers according to the different physical and chemical characteristics of the soil.

The method of controlling the phase metric as a probing signal uses several sources located near the object under study, and the required number of vector measuring sensors of the electric field. The analysis of changes in the phase characteristics of the transfer function [45] has a number of significant advantages over the amplitude methods for fixing the parameters of the anomalous components of the electromagnetic field, in particular, it is characterized by increased sensitivity and noise immunity [46], and allows solving the problems of detecting and localizing geodynamic processes in geological media [47], [48].

The papers [49], [50], [51] explain the application of a modification of this phase-metric method in geoelectric control. In this case, the registration of phase characteristics at a fixed position of the source and measuring base, with the possibility of controlling the parameters of the probing signals, is based on the fact that the primary and secondary electric fields are vector quantities.

D. DATA PROCESSING MODELS

1) GENERATIVE ADVERSARIAL NETWORKS (GANs)

One of the main functions of the GAN is to increase the amount of data that is further used to train an intelligent classification system [52], [53]. A data augmentation strategy based on machine learning algorithms is of particular importance to us. Experiments on drilling rigs are quite expensive. It is impossible to deliberately trigger processes that lead to the destruction of aggregates in an amount sufficient for adequate training of the neural network. However, the traditional GAN [54], [55] has several drawbacks such as mode collapse, gradient disappearance, etc., which reduces the quality of generated samples. Based on this, in order to eliminate shortcomings in the GAN, in a number of works its improved model is proposed [56], [57]. Consider the most promising GAN modifications for solving our problem.

Lin et al., in general. [58] proposed an improved multiscale residual GAN (MsR-GAN) model to obtain fakehigh-quality samples in addition to the experimental results of studies on the performance of failed bearings. The authors have developed a hybrid loss function that improves the classification efficiency of unbalanced failures.

Gao et al. [56] used the ASM1D-GAN method, consisting of a one-dimensional convolutional neural network (1D-CNN), GAN and a fault classifier, to diagnose faults in industrial equipment.

Bo et al. proposed an intelligent diagnostic method based on a generative adversarial network (GAN). A personalized intelligent diagnostic model was created for individual machines. The results showed that this method does not require real fault patterns and provides high diagnostic accuracy. [57].

In [62], [63], [64], and [65], the authors proposed a method for diagnosing faults in rolling bearings based on an improved GAN. As a basis, they used a vibrational signal combined with a continuous wavelet transform capability for non-stationary signal processing and a semi-stationary generation adversarial network (SSGAN) including an image processing and recognition function. The results showed that the fault diagnosis method, combined with the continuous wavelet transform and improved GAN, can provide a higher accuracy than other mainstream diagnostic methods.

2) CAPSULAR CONVOLUTIONAL NEURAL NETWORKS

Capsule networks (CapsNet) proposed by Sabur et al. [61] have had a significant impact on the field of deep learning. Unlike conventional convolutional networks (CNNS), capsule networks maintain orientation relationships between objects. We are primarily interested in the order of the objects,

which does not allow us to use conventional CNNS. The original capsule network model was first applied to images by Hinton, G. E. et al. [67] and this model is our base. However, taking into account the specifics of the problem, its direct use needs improvement.

For automatic recognition of heart diseases by ECG, a one-dimensional network of deep capsules 1D-CADCapsNet was developed [68]. The authors of the work adapted the basic model for processing one-dimensional ECG signals. In addition, the model was supplemented with additional layers. An extremely high accuracy of up to 99.44% has been achieved.

Lalonde proposed the SegCaps network for image segmentation, which is a convolutional deconvolutional capsule network for the problem of object segmentation. They extended the idea of convolutional capsules to locally connected routing and proposed the concept of deconvolutional capsules. [69].

Biswal [70] modified the network, they describe a version of capsules in which each capsule has a logistic unit to represent the presence of an object and a 4×4 matrix that can learn to represent the relationship between that object and the viewer. The authors integrate internal skip connections and a deconvolutional capsular block into a deep M-CapsNet to transform information from every other child into the corresponding parent capsule at every step for efficient semantic segmentation.

E. MAIN CONCLUSIONS INTRODUCTION

1. The transition of the bit between rocks with different properties and the occurrence of self-oscillations in the drill string can lead to damage or even failure of the entire drilling rig.

2. Due to the wear of the bits, 65% of the total number of accidents occur. Equipment failure and increase, in connection with this, downtime of the drilling rig range from 2 to 10% of the cost of the well.

3. Currently used methods that allow real-time determination of the transition of the bit between different rocks with different properties have an accuracy of 70-96%.

4. The phase-metric method has a number of significant advantages over the amplitude methods for fixing the parameters of the anomalous components of the electromagnetic field, in particular, it is characterised by increased sensitivity and noise immunity. Its use together with CapsNet has good prospects for realizing trouble-free operation of the drill string and the bit.

II. MATERIALS AND METHODS

A. DRILLING RIG

We used an Atlas Copco water well drilling rig model T3W. PDC bits and tricone bits were used for drilling (tricone bit), which is universal for rocks of various hardness. This unit allows you to make wells up to 450 meters deep. Average weight in bit 100 êN, angular speed from 20 to 120 rpm.

Phase-metric method of geoelectric control

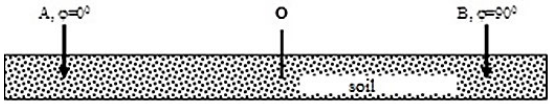

FIGURE 2. Sensor layout.

The geological section can be represented as a dynamic link H(p, Δu), in which the probing electrical signal is converted X(p, Δu), specified in the operator form into a registered electrical signal Y(p, Δu) in the operator form. For this reason, you can get:

$$H\,(p,\,\Delta u) = \frac{\left|Y\,(\rho,\,\Delta u)\,e^{j\varphi_Y(p,\Delta u)}\right|}{\left|X(\rho,\,\Delta u)e^{j\varphi_X(p,\Delta u)}\right|} = \frac{|Y\,(p,\,\Delta u)|}{|X(p,\,\Delta u)|}\,e^{j\Delta\varphi(p,\Delta u)} \tag{1}$$

where φ - signal phase, p – Laplace operator, Δu – strain tensor characterizing the compression and change in the shape of a soil unit. $\Delta\varphi(p,\,\Delta u)$- phase difference of the probing and recorded signals:

$$\Delta\varphi\,(\mathrm{p},\,\Delta u) = \varphi_Y\,(\mathrm{p},\,\Delta\mathrm{u}) - \varphi_X\,(\mathrm{p},\,\Delta\mathrm{u})\,.$$

Accordingly, by changing the phase difference of the signals, one can judge about changes in the electrical characteristics of the controlled medium through which the bit passes, and, therefore, that the bit passes through the boundary between underground rocks with different physical properties.

It follows from the expression obtained that soil control during drilling can be carried out by tracking both the module and the argument (phase) of the recorded geoelectric signals (since the parameters of the sounding signals are constant and known).

In the simplest case, two point sources A, B and one measuring sensor O, located along the line AB and at equal distances from the sources, can be used. Point sources A and B form probing signals shifted in phase by $\pi/2$ relative to each other (Figure 2).

Each of the point sources generates an electric field signal at the point O of the following form:

$$\vec{E}_{AX} = \vec{E}^{\,0}{}_{AX} + \Delta\overline{E}_{AX}, \rightarrow E_{BX} = \vec{E}^{\,0}{}_{BX} + \Delta\overline{E}_{BX}, \tag{2}$$

where $\vec{E}^{\,0}$ - electrical signal recorded before the bit plunged into the ground; $\Delta\overline{E}$ - anomalous component of the electric field caused by the presence of a bit in the soil, causing a change in the electrical characteristics of the soil.

Moreover, the electrodes can be located not only along the line, but also be distributed on the plane. In the latter case, we have the opportunity to track the immersion of the bit in a three-dimensional space, and the accuracy of determining the characteristics of underground rocks increases [3]. The registration of phase characteristics at a fixed position of the source and the measuring basis, with the possibility of controlling the parameters of the probing signals, is based on the fact that the primary and secondary electric fields are vector quantities [4].

The phasometric geoelectric method has increased accuracy and sensitivity to changes in the state of the object under control, which is unattainable using standard amplitude methods (for example, logging while drilling or various modifications of the resistivity method). This is achieved through the initial installation and positioning of radiating and receiving point grounds, the use of original algorithms and methods for generating probing signals to create a multiphase physical field of the desired structure in the controlled area, recording measuring signals, as well as processing and interpreting the information contained in them. Also, among the advantages of the method in relation to the problem being solved, it should be noted its large range and depth, achieved, in particular, due to the use of the low-frequency range, as well as the fact that this method belongs to the class of non-destructive testing methods and does not require the system to be placed directly on the elements and drilling rig structures. However, among the limitations of this method, one should single out the need to solve the problems of identifying extremely small geodynamic changes in the near-surface zones of the geological environment and the initial signs of the development of geotechnical processes. In this aspect, it becomes relevant to solve the problem of increasing the noise immunity of such systems from the influence of interference of natural and artificial origin, as well as increasing the spectral purity of the synthesized signals. To solve this problem, in the future it is proposed to use modulated signals with the expansion of their spectrum as probing signals, as well as to provide hardware approaches to compensating or attenuating the distortions of the generated signals.

B. DESCRIPTION OF THE EXPERIMENT

To assess the possibility of using the phase-metric method in the problems of soil monitoring during well drilling, a full-scale study of the process of the bit passing through underground rocks with different electrical characteristics during drilling of wells in water was carried out. For this, an experimental setup was created (Figure 3), which sources of probing signals, devices for measuring and recording signals in the environment, and a device for includes: processing geodynamic data.

Figures 4 and 5 show the scheme for organizing a full-scale experiment. Electrodes A and B are for input signals with a phase difference of 900 electrodes, M1M2M3N1N2N3 are for output resulting signals.

When using multipole systems of geodynamic control at registration points (M1-M4, N1-N4), one deals with an elliptically polarized geoelectric field. In this case, vector sensors to measure the electric field with the same indices form pairs, the signals of each of which are sent to the measuring system for processing. Data processing of recorded geoelectric signals involves the formation of their difference signal (to filter common-mode noise), its amplification, detection relative to the reference signal, and low-frequency filtering. The principle of registering the phase structure of the geoelectric field at an arbitrary receiving point is illustrated in [3].

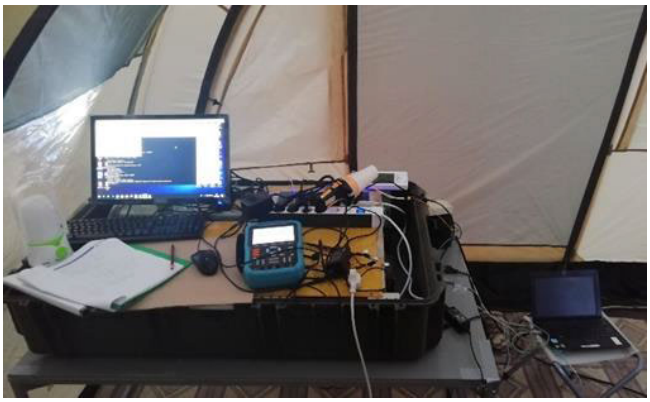

FIGURE 3. Laboratory equipment.

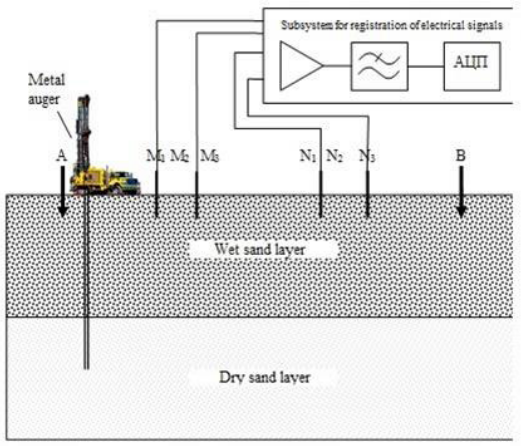

FIGURE 4. Scheme of the organization of the experiment.

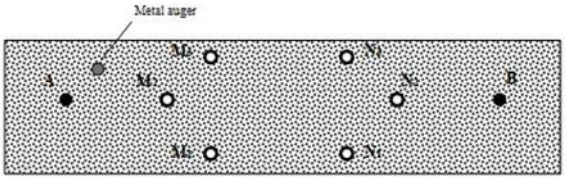

FIGURE 5. Location of electrodes, top view.

As emitting and receiving electrodes, with the help of an artificial electric field was created and recorded, brass rods 1 m long and driven into the ground were used. The frequency of the probing electrical signals was 166 Hz, the amplitude was 500 V, and the shape was harmonic. Digital generation and signal processing were carried out using the E-502-P-EU-D multifunctional ADC/DAC module, which is a data acquisition system based on USB and Ethernet interfaces (Figure 6). The registration of changes in the electric field was carried out with an ADC sampling frequency of 10101 Hz.

To control the seismic background during the measurements, a network of several highly sensitive digital short-period seismometers ZET 7156 (Figure7) was used, designed to measure the values of vibration velocity, allowing instant

FIGURE 6. Appearance of the multifunctional ADC/DAC module E-502-P-EU-D.

FIGURE 7. Appearance of the seismometer ZET 7156.

measurement of vibration velocity in three spatial coordinates (X, Y, Z).

To assess the possibility of using the phase-metric method in the problems of soil monitoring during well drilling, a full-scale study of the process of the bit passing through underground rocks with different electrical characteristics during drilling of wells in water was carried out. For this, an experimental setup (Figure 1) was created, which includes: sources of probing signals, devices for measuring and recording signals in the environment, and a device for processing geodynamic data.

In this case, the following parameters of the experimental setup were used: the distance between the emitting electrodes - 800 m; the distance between receiving electrodes M1N1 – 700 m, the distance between receiving electrodes M2N2 – 600 m, the distance between the receiving electrodes M3N3 – 500 m, the distance between the receiving electrodes M4N4 – 400 m, frequency of probing harmonic electrical signals - 166 Hz, amplitudes of probing harmonic electrical signals – 500V; ADC sampling rate – 10101 Hz.

During the research, a 250 m well was drilled. During drilling, changes in the phase characteristics of electrical signals were recorded (Figure 8).

C. DATA PROCESSING TOOLS

The Python 3.9.13 and PyTorch 1.13.1 libraries were used to develop the algorithm. The experimental platform was

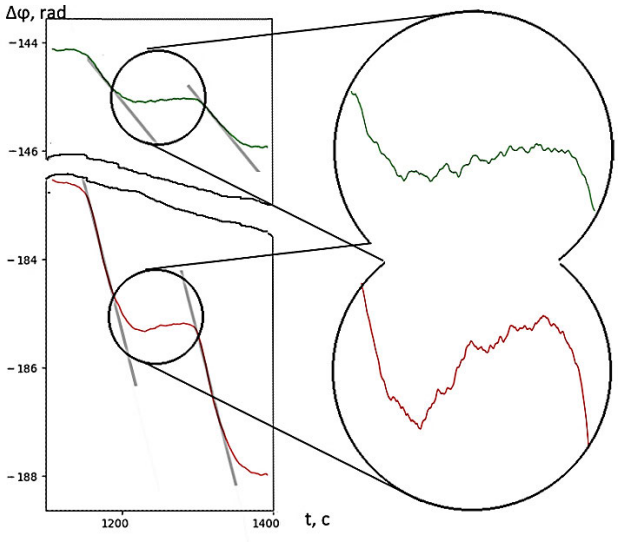

FIGURE 8. Graph of the change in the phase characteristics of electrical signals from the bit at two registration points.

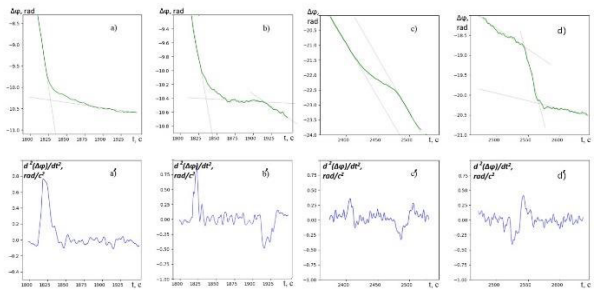

FIGURE 9. Types of graphs of changes in the phase characteristics of electrical signals.

configured with an Intel Core i7-9700K processor, GeForce RTX 2070 GPU, and 64GB of RAM.

D. SIGNAL PREPROCESSING

The change in the phase characteristics of the signals provides information on the depth of drilling and the electrical characteristics of the layers of underground rocks in which the bit is immersed, which makes it possible to judge the degree of moisture saturation of the underground rocks. When the bit moves in a homogeneous medium with constant moisture saturation and with a constant linear speed, the graph of the dependence of the phase transition on time will be linear. Changing the moisture content and characteristics of underground rocks leads to a change in the shape of the graph. The idea of the method is to determine the processes currently taking place at the interface between the bit and underground rock according to the type of graph (Figure 8).

In Figure 9 a) shows the transition of the bit from one rock formation to another. The graph shows the process of a smooth transition from one linear relationship to another.

In Figure 9 b) transition of the bit from one rock formation to another with a change in the mode of rotation of the bit.

In Figure 9 c) the movement of the bit into a layer with a denser inclusion.

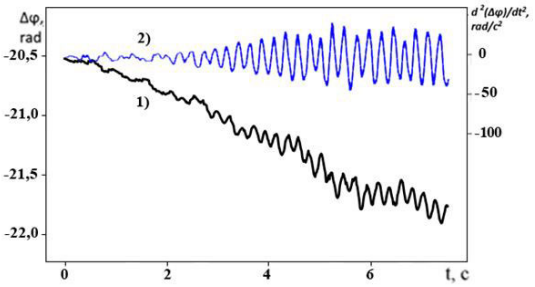

FIGURE 10. Development of self-oscillations of the drill string.

In Figure 9 d) the movement of the bit in a layer with a less dense inclusion. It could be a bit hitting a cavity.

Figure 9 a′) shows the second derivatives of the functional dependencies shown in Figure 9 a). All oscillations occur near the zero axis, which makes it possible to abstract from the uniform movement of the bit inside a homogeneous layer and highlight transient processes. The resulting graphs are more suitable for further processing using a convolutional neural network.

In Figure 9 b′) the transition of the bit from one rock formation to another with a change in the mode of rotation of the bit. Two characteristic peaks are observed.

In figure 9 c′), when the bit moves into a layer with a denser inclusion, in contrast to the graph in Figure 9a′) the maximum passes sharply into a minimum.

In Figure 9 d′) the movement of the bit in a layer with a less dense inclusion. this graph is similar to the previous one. The difference is that the local minimum comes first.

Self-oscillations can randomly occur in the drill string. Often this process is started due to a damaged bit, but in the case of an undamaged bit, the process can take place. This can lead to rig failure and it is important to stop this process as soon as possible [2].

In Figure10. shows how the resulting self-oscillations look on the graph of the change in the phase characteristics of electrical signals (Figure 10.1) and the second derivative of it (Figure 10.2). Drilling was carried out to a depth of 140 meters using a 3-blade PDC bit. Self-oscillations often occur in a drill string using these types of bits [2].

The graph clearly shows the emerging periodicity of the ongoing process. A stable drilling process, represented by small fluctuations along a certain line, turns into an oscillatory process, reaching a maximum amplitude in a short period of time. In the figure, this process is developed in just 8 seconds. The last two seconds are already formed self-oscillation. Moreover, a change in the amplitude of self-oscillations in the future may indicate the inhomogeneity of the material inside which drilling is carried out, or damage to the bit itself.

E. CONVERTING GRAPHS TO 2D VIEW

In order to use 2D-CapsNet for the analysis of phasometric data, the authors of the article made a number of transformations (Figure 11). According to the second derivative of the

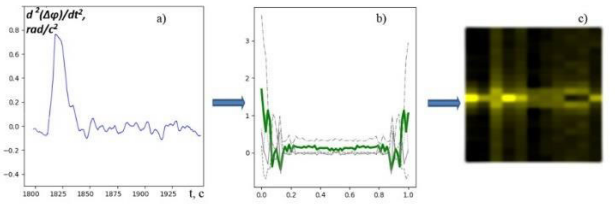

FIGURE 11. Frequency spectrum plot.

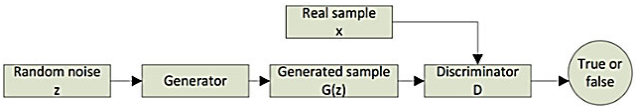

FIGURE 12. GAN structure.

functional dependence (Figure 11.a) of the phase-metric signal, 32 frequency spectrum graphs were built (Figure 11.b). The scipy.fftpack python library was used to create them. The signal was split into 32 windows with 80% overlap. All abscissas of the frequency spectra are converted to the interval from 0 to 1 by the linspace command of the Python Numpy library. A heat map was built according to the frequency spectrum graphs. Each graph is a column in the image (Figure 11.c).

F. GENERATIVE ADVERSARIAL NETWORKS

To stop the oscillatory process in the drill string, it is necessary to change the mode of operation. The problem with tracking fluctuations is that this process happens randomly and it is difficult to collect the necessary amount of data to train the neural network. To obtain a set of data of the required volumes, a significant amount of time is required to monitor the operation of the drill string. To increase the training dataset, the authors used a GAN (Figure 12).

The GAN architecture consists of a generator and a discriminator configured to work against each other.

In each GAN training cycle, a noise variable z occurs randomly [67]. On this basis, signals G(z) are synthesized. After receiving information about the generated signals and raw some detected samples x, the neural network D evaluates the probability that the input data is real samples. Also, G is going to generate fake data that can deceive D as much as possible and obtain a confidential connection. Both models are updated to start the next cycle. This process can be described by the GAN loss function formula (3)

$$\min_{G}\max_{D} E_{x\sim P_{da}}[logD(x)] + E_{z\sim P_g}[log(1 - D(G(z)))] \tag{3}$$

where P_{da} and P_g - the distribution of the real sample over x and the prior distribution of the noise variable z, respectively. The task of the training generator is to minimize the second term of formula (3), and the discriminator is to maximize the objective function in order to obtain the maximum log-likelihood by optimizing between the synthesized sample and

TABLE 1. Layers of the GAN generator model.

N	Layer Name	Filter × Kernel Size	Other Params	Output Size
1	Z	-	-	100
2	Deconv	512 × 3 × 3	strides = 2 act = PReLU	4 × 4 × 512
3	Deconv	256 × 3 × 3	strides = 2 act = PReLU	8 × 8 × 256
4	Deconv	128 × 3 × 3	strides = 2 act = PReLU	16×16×128
5	Deconv	64 × 3 × 3	strides = 2 act = PReLU	32×32×64
6	Deconv	3 × 3 × 3	strides =1 act = PReLU	32×32×3

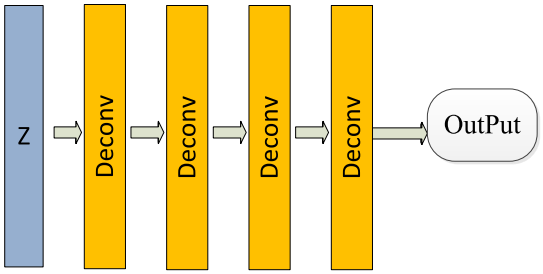

FIGURE 13. Block representation of the GAN generator network model.

real data. After adversarial training, the generated samples G fully correspond to the distribution of real samples ($P_{da} = P_g$).

As shown in Figure 13, the input of G is a 100D random noise z subject to Gaussian distribution, with the mean value of 0 and a standard deviation of 1. Firstly, z is projected and reshaped into 4 × 4 × 512 size feature maps. Then, these feature maps are transformed into Conv representations by 4 deconvolutional (Deconv) blocks (Table 1). Each block includes a Deconv layer with 3 × 3 kernel size, a batch normalization (BN) layer used to accelerate model training and improve its generalization ability, and a PReLU activation layer.

$$\mathrm{PReLU}(x) = \begin{cases} \mathrm{x}, \text{ if } \mathrm{x} > 0 \\ \alpha_i \mathrm{x}, \text{ if } \mathrm{x} \leq 0 \end{cases} \tag{4}$$

where i represents the index of channel, and α_i is a learnable parameter. We use the channel-shared version of PReLU. Here, channel-share means the coefficient is shared by all channels of one layer. The initial value of α_i is assigned with a value of 0.25. The values of bk are updated by back propagation and optimized simultaneously in all layers [71].

Input D receives an image of 32 × 32 × 3 image (Figure 14). The image passes through three convolutional layers and two MaxPool layers, the parameters of which are shown in Table 2. Then comes the layer batch normalization (BN) layer used to accelerate model training and improve its generalization ability. The reduction module is mainly used for further dimension reduction. The following is a dropout layer to prevent the model from overfitting. Finally, two

TABLE 2. Layers of the discriminator GAN model.

N	Layer Name	Filter × Kernel Size	Other Params	Output Size
1	Input Layer	-	-	32×32×3
2	Conv2D	32 × 3 × 3	strides = 1	32×32×32
3	MaxPool	64 × 3 × 3	strides = 2	15×15×64
4	Conv2D	64 × 1 × 1	strides = 1	15×15×64
5	Conv2D	96 × 3 × 3	strides = 1	13×13×96
6	MaxPool	64 × 3 × 3	strides = 1	11×11×192
7	BN	-	-	11×11×192
8	Reduction module	-	-	5 × 5 × 576
9	DropOut	-	-	5 × 5 × 576
10	FC layer	-	-	14400
11	FC layer	-	-	1
12	OutPut	-	-	1

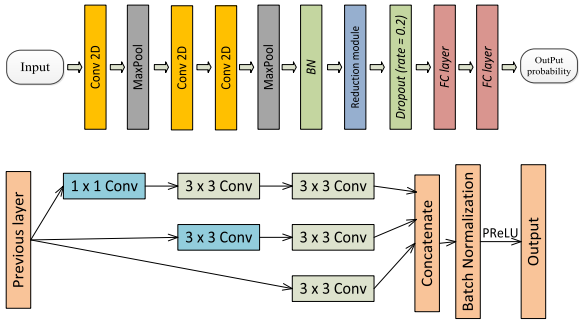

FIGURE 14. Block representation of the Discriminator GAN network model.

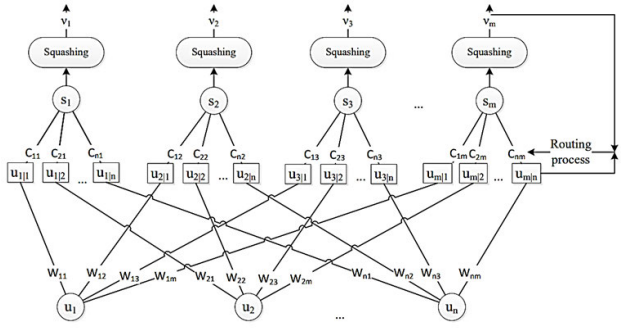

FIGURE 15. Dynamic routing algorithm in CapsNet.

fully connected (FC) layers are used to output the predicted probabilities.

When training GAN, the following hyperparameters are used: Batch size - 64; Epochs - 150; Learning rate - 0.0001; Optimizer - Adam optimizer.

G. CAPSULE NETWORK

The essence of the CapsNet algorithm is to convert neurons from a scalar to a vector. This is necessary to reduce information loss and improve the ability to extract features.

We use the non-linear squashing function given by

$$v_j = \frac{\|s_j\|^2}{1 + \|s_j\|^2} \frac{s_j}{\|s_j\|}, \tag{5}$$

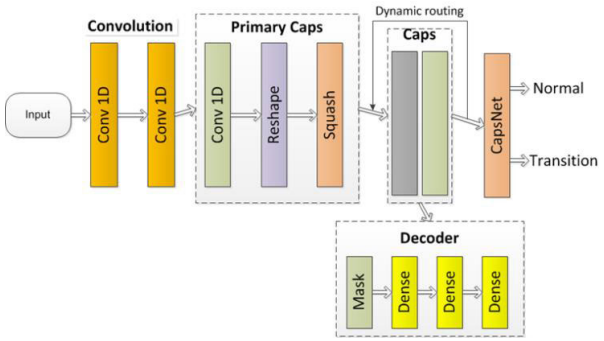

FIGURE 16. Block representation of the 1D-CapsNet network model for automatic determination of the nature of changes in drilling conditions.

where υ_j is the vector output of capsule j and S_j is its input. The final output vector υ_j is obtained by a nonlinear mapping of S_j

The output vector S_j is the weighted sum of $u_{j|i}$

$$s_j = \sum_i C_{ij} u_{j|i}, \tag{6}$$

where C_{ij} is the coupling coefficients determined by the dynamic routing algorithm. These coefficients represent a probability distribution for the low-level capsule output to which they are sent to high-level capsules.

$$\underset{j|i}{u} = W_{ij} u_i, \tag{7}$$

where u_i is the i-th neuron in the upper layer, W_{ij} is the weight matrix, $u_{j|i}$ is the prediction vector:

$$C_{ij} = \frac{exp\left(b_{ij}\right)}{\sum_k exp\left(b_{ik}\right)}, \tag{8}$$

$$b_{ij} = b_{ij} + v_j u_{ji}, \tag{9}$$

where the is j denotes the j-th output neuron. C_{ij} is b_{ij} are determined by the dynamic routing algorithm.

For classification, we used a capsule network (CapsNet). A signal is applied to the input of the network, and abstract representations are created at the output. Unlike Convolutional Neural Networks (CNNs), Capsule Networks store object parameters such as the object's orientational (rotational and translational) relationships.

H. 1D-CapsNet

In this article, a one-dimensional model of the 1D-CapsNet capsule network was developed for automatic recognition of processes occurring during drilling and monitoring using the phase-metric method. The original capsule network model is shown in the figure. (Figure 16)

The ReLU activation function is defined as follows:

$$\mathrm{ReLU}(x) = \begin{cases} \mathrm{x}, \text{if } \mathrm{x} > 0 \\ 0, \text{if } \mathrm{x} \leq 0 \end{cases} \tag{10}$$

When training 1D-CapsNet, the following hyperparameters are used: Batch size - 128;

TABLE 3. Layers of the 1D-CapsNet model and various layer parameters (for a group of segments 51.4 s).

N	Layer Name	Filter × Kernel Size	Dim × Num (capsules)	Other Params	Output Size
1	Input Layer	-	-	-	514×1
2	Conv1D	32 × 5	-	strides = 2 act = ReLU	255 × 32
3	Conv1D	64 × 3		strides = 1 act = ReLU	253 × 64
4	Primary Caps (Conv1D)	512 × 3	16 × 32	strides = 2	126 × 512
5	Primary Caps (Reshape)				4032 × 16
6	Primary Caps (Squash)				4032 × 16
7	Caps (CapsuleLayer)		32 × 2	num_routing = 3	2 × 32
8	Decoder				514 × 1
9	CapsNet				2

Epochs - 30; Alpha (reconstruction) - 0.2; Number of routing - 3; Shift fraction - 0.1; Optimizer - Adam optimizer. The 1D-CapsNet model contains convolutional layers, a Primary Caps layer, and a Caps layer. The signal from the experimental setup was fed to the network input, which was pre-processed according to the "Signal Pre-Processing" item. The input layer dimensions were set to 514 × 1, which covered a time range of 51.4 seconds in 0.1 second increments (Table 3). The input signals were passed through two layers of one-dimensional convolution (Conv1D) with the parameters shown in Table 3. large, this means that the capsules have found the important features they are looking for in the Primary Caps block. The reshaping layer, which was located after the convolutional layer, was used to transform the array of feature maps into the corresponding vectors. Then, in the last step of the Primary Caps layer, the squash function was used to ensure that the lengths of all vectors were between 0 and 1. The squash function for vector S was defined by the formula:

$$Squash(S) = \frac{\|S\|^2}{1 + \|S\|^2} \frac{\|\mathrm{S}\|}{1 + \|\mathrm{S}\|'} \tag{11}$$

the result of the function is a probability that indicates the presence of waveform features, so it cannot be greater than 1. The squash function stores detailed information about the signals during network training. The Caps layer contained two capsules for determining the transition of the bit through layers of rock with different properties, which represent the Normal and Transition classes and have a size of 32. Information about a particular object is stored in the activation vector dimension. This allows CapsNet to demonstrate high performance. In this part of the network, a dynamic routing algorithm was implemented.

Capsule stand to predict the yield of capsules in the next layer. The capsules prediction output generated a cluster of prediction vectors.

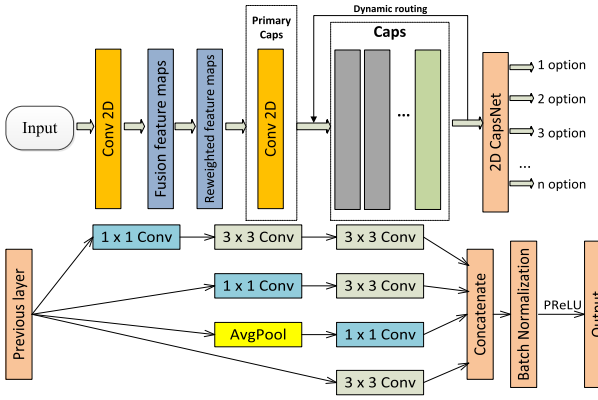

FIGURE 17. Block representation of the 2D-CapsNet network model for automatic determination of the nature of changes in drilling conditions.

TABLE 4. Layers of the 2D-CapsNet model and various layer parameters (for a group of segments 51.4 s).

N	Layer Name	Filter × Kernel Size	Dim × Num (capsules)	Other Params	Output Size
1	Input Layer	-	-	-	32×32×3
2	Conv2D	128 × 3 × 3	-	strides = 2 act = PReLU	16×16×128
3	Fusion feature maps				16×16×128
4	Reweighted feature maps				16×16×128
5	Primary Caps (Conv2D)	128 × 3 × 3	15×15×8×16	strides =2	15×15×128
6	DigitCaps		16×n		n×16
7	2D-CapsNet				n

The mean of the prediction vectors was then calculated to find the distances between the mean vector and the prediction vectors. This process calculates the correspondence between each predictive vector and the mean vector. The predicted vector weight has been updated to reflect this distance measure. Vectors that were far from the mean received a small update, and predicted vectors that were close to the mean received large updates. We repeated the routing process 3 times to update the network settings.

I. 2D-CapsNet

In this article, in addition to the one-dimensional model, a two-dimensional model of the 2D-CapsNet capsule network was developed for automatic recognition of processes occurring during drilling and monitoring using the phase-metric method. (Figure 17).

When training 2D-CapsNet, the following hyperparameters are used: Batch size - 50; Epochs - 30; Learning rate - 0.0001; Optimizer - Adam optimizer.

The general structure of the proposed 2D - CapsNet model is presented in Table 4. After the first Conv2D layer, 32 × 32×3 input images are transformed into 16 × 16×128 feature maps, followed by a feature enhancement network (feature map). It consists of four branches, each of which

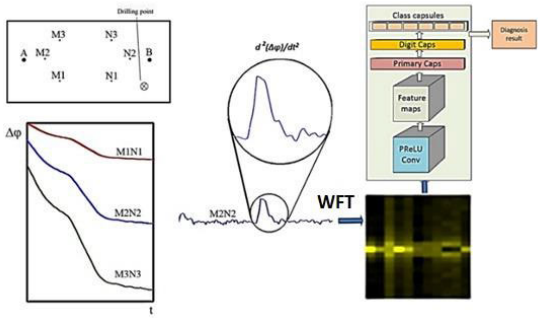

FIGURE 18. Scheme of the proposed approach to identifying the state of the drill string and the bit based on the WFT-2D-CapsNet method.

enhances the features characterizing bit damage and self-oscillations in the drill string (Figure 17).

The basic CapsNet classifier consists of three parts:

1. The Primary capsule layer (Primary Caps), which is an improved Conv2D layer in which 128 channels are converted into 16 vectors of length 8;

2. The digital capsule (Digit Caps) layer that uses the dynamic routing algorithm to transform the output of Pimarycaps into n 16-D capsule vectors, where the algorithm loops three times, and n represents the number of fault types;

3. In the capsule layer class, the length of each capsule vector represents the possibility of each type of malfunction, i.e. the L2 norm the capsule vector determines the final diagnostic result.

J. SUGGESTED APPROACH

The authors of the article propose an algorithm for detecting the state of the drilling system, leading to its damage (Figure 18):

Step 1: The signal of the change in the phase characteristics of the electrical signals coming from the transmitter of the experimental setup is processed, and the second derivative is found from it.

Step 2: Using the Fourier Transform (WFT), the resulting second derivative plot is converted into a 2D RGB image of a specific size.

Step 3: These sample images are divided into two parts according to a certain proportion: training set and test set. The CapsNet model is trained.

Step 4: The test set is injected into the trained CapsNet model to diagnose abnormal conditions.

Step 5: Diagnostic results are displayed.

III. RESULTS AND DISCUSSION

A. INDICATORS FOR DATA PRODUCTION AND EVALUATION

In the process of processing the results of the experiment, we will consider separately the translational and oscillatory motion of the bit. The first process is rather extended in time. For measurements, we take a time interval of 51.4 seconds with a frequency of taking indicators of 0.1 s.

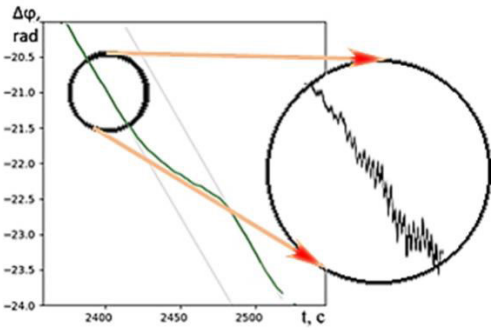

FIGURE 19. Periodic process on the diagram of changes in the phase characteristics of an electrical signal.

TABLE 5. Number of samples used to determine transition of a bit from one layer of rock to another.

CHART TYPE	CHART CLASSIFICATION	TRANSITION DETECTION BIT BETWEEN LAYERS
Bit transition between layers	155	155
The movement of the bit in a homogeneous layer	160	
Bit motion in a layer with a denser inclusion	112	
Bit movement in a layer with a less dense inclusion or cavity	84	356

Every 10 seconds, a reprocessing process is performed. The small amount of data processed at the same time allows you to work in low latency mode. The oscillatory process is rapidly changing. Its frequency is related to the speed of rotation of the bit, and it takes much less time to determine the necessary characteristics of this process. The determination of the presence of an oscillatory process is carried out for 10 seconds at a frequency of taking indicators of 0.02 seconds. (Figure 19). This process may be repeated periodically, for example, every 2 minutes.

For the first process. To simplify the classification task, two stages of preprocessing were carried out. At the first stage, data samples were selected based on the following considerations: for all graphs in Figure 9, the capture interval is 51.4 seconds at a sampling rate of 10 Hz.

In the second stage, the graphs returned to normal.

The results obtained were used to train the models (see Table 5).

A 5-fold cross-validation method was applied to them. The data was divided into two parts. The training set was associated with the test set as 80% and 20% of all data, respectively. The distribution structure of the training and testing data is shown in Figure 20.

Identification of the transition between different layers of rocks was carried out using binary classification. The first class is the transition of the bit between two different layers, and the second class is any other processes. When training

FIGURE 20. Illustration of the 5-fold method used to evaluate the effectiveness of the proposed method.

TABLE 6. Accuracy of four different deep learning architectures.

Networks	Basic-DCNNs	VGGNet-16	1D-CapsNet	WFT-2D-CapsNet
Accuracy	88,3%	94,8%	98,5%	99,4%

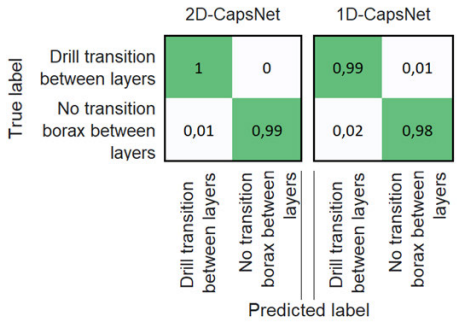

FIGURE 21. Confusion matrices for the 1D-CapsNet and WFT-2D-CapsNet methods.

and testing methods, graphs of a fully completed process of transition between stable states were used.

Four methods were used: Basic-DCNNs, VGGNet-16, 1D-CapsNet, and WFT-2D-CapsNet. The first two have performed well in image classification. These methods can be studied in detail in Lee et al. [72]. The accuracy of detecting a bit transition between two rock layers with different properties is shown in Table 6.

For a more detailed explanation, Figure 21 shows a comparison of the confusion matrix for the two highest performing of the four algorithms. These are two types of capsular neural networks: 1D-CapsNet and WFT-2D-CapsNet, developed by the authors of the article.

On the basis of the results, we see that the WFT-2D-CapsNet method performs better.

We singled out two more classes: bit movement in a layer with a denser inclusion and bit movement in a layer with a less dense inclusion or cavity. For classification, the WFT-2D-CapsNet method was used. Figure 22 shows the confusion matrix for this method.

For the second process.

The features of the second sample are that the fluctuations of the drilling system occur involuntarily and it is quite

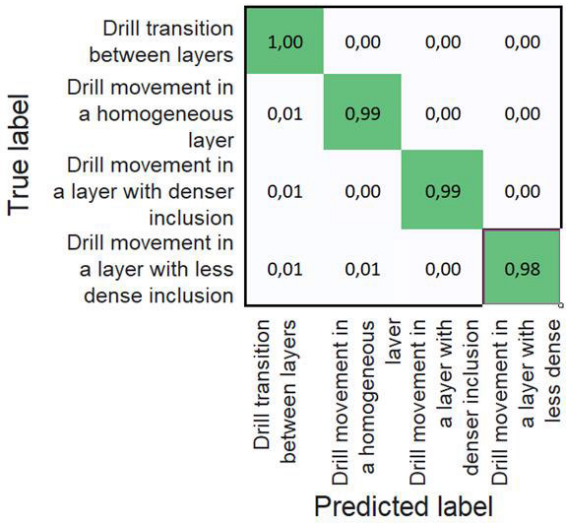

FIGURE 22. Confusion matrix for the WFT-2D-CapsNet method.

TABLE 7. Number of measurement series used to determine the type of vibrations that occurred in the drilling system.

Chart type	Chart classification
Movement of an intact bit with vibrations	20
Movement of a damaged bit with vibrations	8

difficult to track them. This explains the small number of signal samples (Table 7). The damaged bit had significant wear and large chips on 20% of the cutting elements of the PDC bits.

The experiments were carried out in series of 5 to 20 separate measurements, 10 s each, with a difference between measurements of up to 2 min. The preprocessing steps are described in the Suggested Approach section of the Materials and Methods chapter.

The initial processing of a series of experiments is shown in Figure 23. According to the diagram of the second derivative Figure 23(b), you can visually assess the degree of wear and damage to the bit. The more chaotic the graph, the more damaged the bit. On the frequency response of a series of experiments in Figure 23(c) clearly shows the frequency of oscillations generated in the drill string and the bit (the highest maximum on the graph).

To increase the sample size, we use GAN. The structure of the GAN is given in the Materials and Methods chapter. To determine the quality of the GAN proposed by the authors, the Frechet Inception Distance (FID) metric was used. You can see more about it in the work] Lee et al. [72].

Three methods were used for comparison with corresponding FID results:

Image transformation (IT) including (width shift, height shift, horizontal flip, vertical flip, rescale) – 0.637 ± 0.022;

The GAN used in the work is 0.693 ± 0.021;

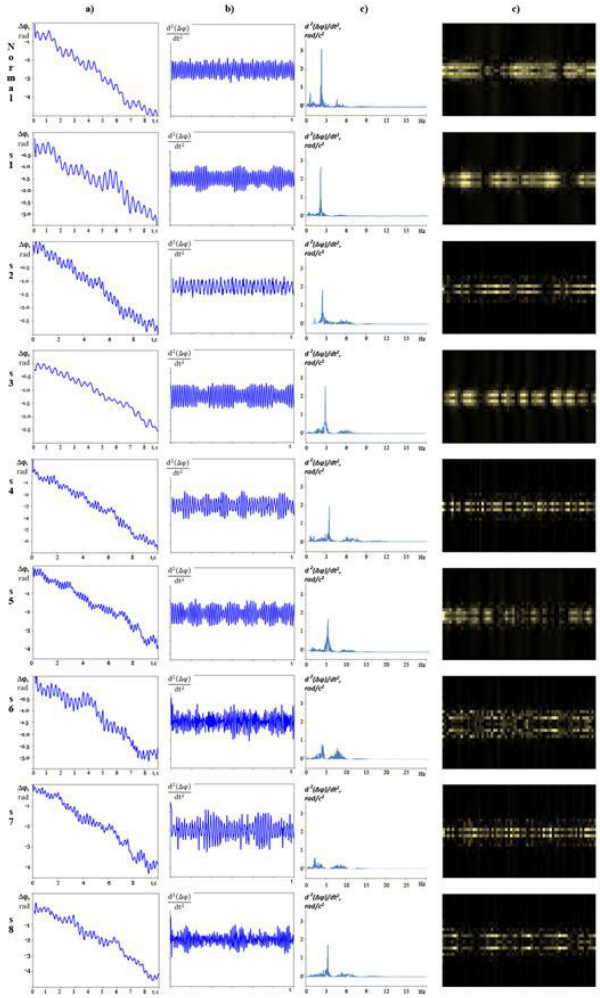

FIGURE 23. Initial processing of a series of experiments. a) diagram of changes in the phase characteristics of the electrical signal; b) diagram of the second derivative of a; c) frequency characteristics of a series of experiments (Fourier transform); d) 2D model of each series.

GAN without Reduction module (instead of this module, a Conv2D layer with a 3×3 core is inserted) - – 0.714 ± 0.021.

The FID values were calculated by averaging the original 400 samples and the generated 400 samples of three types. GAN training periods are set to 150. Optimizer is Adam. It can be seen that the FID values for IT are minimal because it only performs a geometric transformation but cannot learn the distribution of features in the original data. The GAN method we proposed is the second in terms of results, which indicates that the data it generates are closest to the original and have the best quality.

The results of the method are shown in the confusion matrix (Figure 24).

To intuitively understand data differences between different series of experiments, we use the t-SNE algorithm [69]. The data is taken at the WFT-2D-CapsNet class capsule level, as shown in Figure 25.

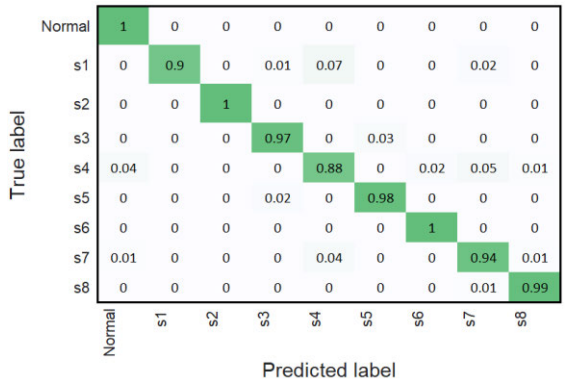

FIGURE 24. Confusion matrix for the WFT-2D-CapsNet method.

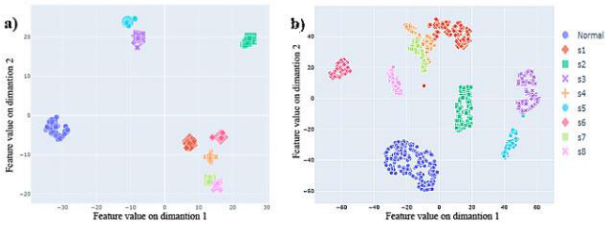

FIGURE 25. Using t-SNE to visualize data at the capsule level WFT-2D-CapsNet: (a) series of samples; (b) generated GAN data.

TABLE 8. Distribution of series of experiments by classes.

Class name	RELEVANT CLASSES
Normal	Normal
1-type damage	S1, S4, S6, S7, S8
2-type damage	S3, S5
3-type damage	S2

As can be seen in Figure 25. The feature distribution of the original and generated samples is almost consistent, indicating that the proposed GAN-based data augmentation strategy can effectively augment imbalanced data. A number of clusters from different samples intersect, which indicates the similarity of bit damage. Combining overlapping clusters, we got 4 classes (Table 8). We are primarily interested in the ordinary class. It's detection accuracy Is 98%.

With an increase in the depth of the well, the oscillation frequency of the drill string and the bit decreases (Figure 26). This changes the 2D model.

We found that WFT-2D-CapsNet starts to err when the training and test samples differ in depth by more than 50 meters. On average, the accuracy decreases by 2% for every 50 meters of difference.

IV. DISCUSSION

In this paper, the effectiveness of using machine learning methods for continuous monitoring of the state of the drill

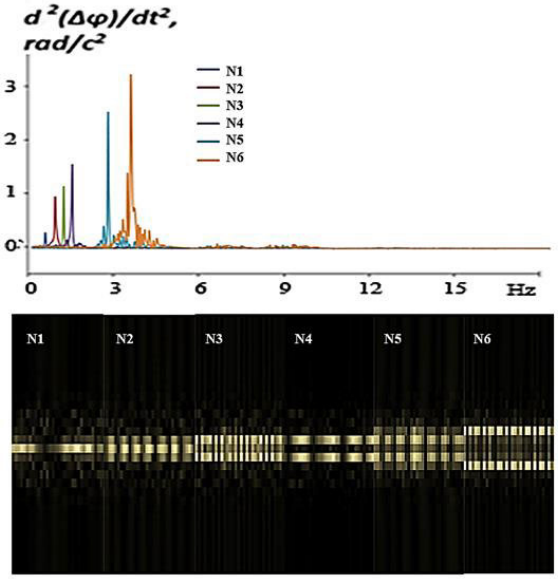

FIGURE 26. Frequency response and 2D model of a series of experiments under the conditions of the resulting vibration in the drilling system in the case of an intact bit at different depths.

string and the bit is shown. As a data source, a phase metric geoelectric experiment all set up was used, which made it possible, firstly, to achieve a low time delay in detecting the state of self oscillation of the drill string and the state of the bit transition through rock layers with different properties, and secondly, the degree of bit wear.

The phase metric geoelectric control method used has increased accuracy and sensitivity to changes in the state of the controlled object, which is unattainable using standard amplitude methods. At the same time, it is not required to place the system directly on the elements and structures of the drilling rig.

The limitations of the method are: the need to solve the problems of identify in extremely small geodynamic changes in the near-surface zones of the geological environment, the need to identify the initial signs of the development of geotechnical processes, and the solution of the problem of increasing noise immunity.

Approximate sound in depth - up to 1.5 km. In this case, the electrodes must be spaced twice as far as the depth. The installation was tested frequencies of the probing signal - up to kilohertz Voltage - 1-2 kilovolts Power - 0.5 - 1 kW.

The results of modern rock surveys based on measurement-while-drilling (MWD), logging-while-drilling (LWD) and other tools that transmit downhole data collected to the surface in near real time range from 70% to 96 % [74], [75], [76]. The results obtained by us exceeded the best indicators by 2-3%.

A significant result of the research is associated primarily with the machine learning methods developed by the authors of the article, which work on the basis of capsular convolutional neural networks 1D-CapsNet and 2D-CapsNet.

When conducting a comparative analysis with convolutional neural networks (CNN), their accuracy is 3-7% lower. As an example, Basic-DCNNs and VGGNet-16 were taken. Among the capsular neural networks developed by the authors, 2D-CapsNet turned out to be more accurate (its accuracy was 99% when determining the bit transition between rock layers). In addition, it uniquely identifies the oscillatory process that has arisen on the drill string. The result of the method is the classification of the operating state of the bit. From our series of observations, we identified 4 classes of such states. At this stage of the study, we are only interested in the first option - a fully serviceable bit. The method proposed by the authors separates this class from other classes with an accuracy of 99%.

A. MAIN LIMITATIONS AND WIDER APPLICABILITY OF THE METHOD

At this stage of the study, the method proposed by the authors of the article can, with a probability of 99%, separate the work of a serviceable bit from a bit with chips on it. In most cases, you can work with such bits for some time. In further work, it is planned to establish a criterion under which the further operation of a damaged bit will be impractical or even dangerous.

We found that WFT-2D-CapsNet starts to make errors when the training and test samples differ in depth by more than 50 meters. We believe that this shortcoming will be eliminated with an increase in the number of experimental samples taken at different depths.

It is planned to expand the research to a well depth of up to 1.5 km.

REFERENCES

[1] L. Lin, H. Guo, F. Guo, Y. Lv, J. Liu, and C. Tong, "A novel domain adversarial time-varying conditions intervened neural network for drill bit wear monitoring of the jumbo drill under variable working conditions," *Measurement*, vol. 208, Feb. 2023, Art. no. 112474, doi: 10.1016/j.measurement.2023.112474.

[2] A. G. Aribowo, R. Wildemans, E. Detournay, and N. van de Wouw, "Drag bit/rock interface laws for the transition between two layers," *Int. J. Rock Mech. Mining Sci.*, vol. 150, Feb. 2022, Art. no. 104980, doi: 10.1016/j.ijrmms.2021.104980.

[3] S. K. Gupta and P. Wahi, "Tuned dynamics stabilizes an idealized regenerative axial-torsional model of rotary drilling," *J. Sound Vib.*, vol. 412, pp. 457–473, Jan. 2018.

[4] U. J. F. Aarsnes and N. van de Wouw, "Axial and torsional self-excited vibrations of a distributed drill-string," *J. Sound Vib.*, vol. 444, pp. 127–151, Mar. 2019.

[5] Y. A. Khulief and H. Al-Naser, "Finite element dynamic analysis of drillstrings," *Finite Elements Anal. Des.*, vol. 41, pp. 1270–1288, Jul. 2005.

[6] B. Besselink, T. Vromen, N. Kremers, and N. van de Wouw, "Analysis and control of stick-slip oscillations in drilling systems," *IEEE Trans. Control Syst. Technol.*, vol. 24, no. 5, pp. 1582–1593, Sep. 2016.

[7] M. Wu, J. Cheng, C. Lu, L. Chen, X. Chen, W. Cao, and X. Lai, "Disturbance estimator and Smith predictor-based active rejection of stick–slip vibrations in drill-string systems," *Int. J. Syst. Sci.*, vol. 51, no. 5, pp. 826–838, Apr. 2020.

[8] Y. A. Khulief, F. A. Al-Sulaiman, and S. Bashmal, "Vibration analysis of drillstrings with self-excited stick–slip oscillations," *J. Sound Vib.*, vol. 299, no. 3, pp. 540–558, Jan. 2007.

[9] B. Besselink, N. van de Wouw, and H. Nijmeijer, "A semi-analytical study of stick-slip oscillations in drilling systems," *J. Comput. Nonlinear Dyn.*, vol. 6, no. 2, pp. 021006-1–021006-9, Apr. 2011.

[10] J. R. Bailey, E. A. O. Biediger, V. Gupta, D. Ertas, W. C. Elks, and F. E. Dupriest, "Drilling vibrations modeling and field validation," in *Proc. IADC/SPE Drilling Conf.* Richardson, TX, USA: OnePetro, Mar. 2008.

[11] S. F. Sowers, F. E. Dupriest, J. R. Bailey, and L. Wang, "Roller reamers improve drilling performance in wells limited by bit and bottom-hole assembly vibrations," in *Proc. SPE/IADC Drilling Conf. Exhib.* Richardson, TX, USA: OnePetro, Mar. 2009.

[12] J. R. Bailey, E. A. O. Biediger, S. Sundararaman, A. D. Carson, W. C. Elks, and F. E. Dupriest, "Development and application of a BHA vibrations model," in *Proc. Int. Petroleum Technol. Conf.* Richardson, TX, USA: OnePetro, Dec. 2008.

[13] F. E. Dupriest, W. C. Elks, S. Ottesen, P. E. Pastusek, J. R. Zook, and C. R. Aphale, "Borehole quality design and practices to maximize drill rate performance," in *Proc. SPE Annu. Tech. Conf. Exhib.* Richardson, TX, USA: OnePetro, Sep. 2010.

[14] X. Liu, N. Vlajic, X. Long, G. Meng, and B. Balachandran, "Coupled axial-torsional dynamics in rotary drilling with state-dependent delay: Stability and control," *Nonlinear Dyn.*, vol. 78, no. 3, pp. 1891–1906, Nov. 2014.

[15] K. Nandakumar and M. Wiercigroch, "Stability analysis of a state dependent delayed, coupled two DOF model of drill-stringvibration," *J. Sound Vib.*, vol. 332, no. 10, pp. 2575–2592, May 2013.

[16] C. Lu, M. Wu, X. Chen, W. Cao, C. Gan, and J. She, "Torsional vibration control of drill-string systems with time-varying measurement delays," *Inf. Sci.*, vol. 467, pp. 528–548, Oct. 2018.

[17] X. Liu, N. Vlajic, X. Long, G. Meng, and B. Balachandran, "Nonlinear motions of a flexible rotor with a drill bit: Stick-slip and delay effects," *Nonlinear Dyn.*, vol. 72, nos. 1–2, pp. 61–77, Apr. 2013.

[18] H. Zhang and E. Detournay, "A high-dimensional model to study the self-excited oscillations of rotary drilling systems," *Commun. Nonlinear Sci. Numer. Simul.*, vol. 112, Sep. 2022, Art. no. 106549.

[19] A. G. Aribowo, R. Wildemans, E. Detournay, and N. van de Wouw, "Drag bit/rock interface laws for the transition between two layers," *Int. J. Rock Mech. Mining Sci.*, vol. 150, Feb. 2022, Art. no. 104980.

[20] F. Zhang, Y. Lu, D. Xie, H. Luo, R. Shi, and P. Zhang, "Experimental study on the impact resistance of interface structure to PDC cutting tooth," *Eng. Failure Anal.*, vol. 140, Oct. 2022, Art. no. 106503.

[21] Z. Huang, D. Xie, B. Xie, W. Zhang, F. Zhang, and L. He, "Investigation of PDC bit failure base on stick-slip vibration analysis of drilling string system plus drill bit," *J. Sound Vib.*, vol. 417, pp. 97–109, Mar. 2018.

[22] A. Toutov, N. Toutova, A. Vorozhtsov, and I. Andreev, "Optimizing the migration of virtual machines in cloud data centers," *Int. J. Embedded Real-Time Commun. Syst.*, vol. 13, no. 1, pp. 1–19, 2022, doi: 10.4018/IJERTCS.289200.

[23] A. Z. Mazen, I. M. Mujtaba, A. Hassanpour, and N. Rahmanian, "Mathematical modelling of performance and wear prediction of PDC drill bits: Impact of bit profile, bit hydraulic, and rock strength," *J. Petroleum Sci. Eng.*, vol. 188, May 2020, Art. no. 106849.

[24] A. V. Toutov, N. V. Toutova, and A. S. Vorozhtsov, "Analysis of data center development problems in the era of digital transformation," in *Model-Driven Organizational and Business Agility* (Lecture Notes in Business Information Processing), vol. 457, E. Babkin, J. Barjis, P. Malyzhenkov, and V. Merunka, Eds. Cham, Switzerland: Springer, 2022, doi: 10.1007/978-3-031-17728-6_6.

[25] K. Miyazaki, T. Ohno, H. Karasawa, and H. Imaizumi, "Performance of polycrystalline diamond compact bit based on laboratory tests assuming geothermal well drilling," *Geothermics*, vol. 80, pp. 185–194, Jul. 2019.

[26] K. U. M. Rao, A. Bhatnagar, and B. Misra, "Laboratory investigations on rotary diamond drilling," *Geotechnical Geological Eng.*, vol. 20, no. 1, pp. 1–16, 2002.

[27] J. Liu, H. Zheng, Y. Kuang, H. Xie, and C. Qin, "3D numerical simulation of rock cutting of an innovative non-planar face PDC cutter and experimental verification," *Appl. Sci.*, vol. 9, no. 20, p. 4372, Oct. 2019, doi: 10.3390/app9204372.

[28] Q. Peng, Y. Zhou, J. Yu, X. Yang, Y. Liu, C. Ma, C. Cheng, and X. Ke, "Study on rock breaking efficiency of special shaped cutters," *IOP Conf. Ser., Earth Environ. Sci.*, vol. 983, no. 1, Feb. 2022, Art. no. 012089, doi: 10.1088/1755-1315/983/1/012089.

[29] Y. Zhao, A. Noorbakhsh, M. Koopialipoor, A. Azizi, and M. M. Tahir, "A new methodology for optimization and prediction of rate of penetration during drilling operations," *Eng. Comput.*, vol. 36, no. 2, pp. 587–595, Apr. 2020, doi: 10.1007/s00366-019-00715-2.

[30] J. Tang, Y. Lu, Z. Ge, B. Xia, H. Sun, and P. Du, "A new method of combined rock drilling," *Int. J. Mining Sci. Technol.*, vol. 24, no. 1, pp. 1–6, 2014.

[31] Y. Zhan and G. Zhang, "An improved Otsu algorithm using histogram accumulation moment for ore segmentation," *Symmetry*, vol. 11, no. 3, p. 431, Mar. 2019.

[32] J. D. Kana, N. Djongyang, D. Raïdandi, P. N. Nouck, and A. Dadjé, "A review of geophysical methods for geothermal exploration," *Renew. Sustain. Energy Rev.*, vol. 44, pp. 87–95, Apr. 2015.

[33] E. Boltachev, "Potential cyber threats of adversarial attacks on autonomous driving models," *J. Comput. Virol. Hacking Techn.*, pp. 1–11, 2023.

[34] A. Malehmir, E. Koivisto, M. Manzi, S. Cheraghi, R. J. Durrheim, G. Bellefleur, C. Wijns, K. A. A. Hein, and N. King, "A review of reflection seismic investigations in three major metallogenic regions: The Kevitsa Ni–Cu–PGE district (Finland), Witwatersrand goldfields (South Africa), and the Bathurst Mining Camp (Canada)," *Ore Geol. Rev.*, vol. 56, pp. 423–441, Jan. 2014.

[35] C. C. Pretorius, M. R. Müller, M. Larroque, and C. Wilkins, "A review of 16 years of hardrock seismics on the Kaapvaal Craton," in *Hard Rock Seismic Exploration*, D. W. Eaton, B. Milkereit, and M. H. Salisbury, Eds. Tulsa, OK, USA: SEG, 2003, pp. 247–268.

[36] M. Urosevic, B. Ganesh, and G. Marcos, "Targeting nickel sulfide deposits from 3D seismicreflection data at Kambalda, Australia," *Geophysics*, vol. 75, pp. 123–132, Sep. 2012.

[37] T. D. Nguyen and K. T. Tran, "Site characterization with 3D elastic full-waveform tomography," *Geophysics*, vol. 83, no. 5, pp. 389–400, 2018, doi: 10.1190/geo2017-0571.1.

[38] S. Udphuay, T. Günther, M. E. Everett, R. R. Warden, and J. Briaud, "Three-dimensional resistivity tomography in extreme coastal terrain amidst dense cultural signals: Application to cliff stability assessment at the historic D-day site," *Geophys. J. Int.*, vol. 185, no. 1, pp. 201–220, Apr. 2011, doi: 10.1111/j.1365-246X.2010.04915.x.

[39] J. Place and A. Malehmir, "Using supervirtual first arrivals in controlled-source hardrock seismic imaging—Well worth the effort," *Geophys. J. Int.*, vol. 206, no. 1, pp. 716–730, Jul. 2016, doi: 10.1093/gji/ggw176.

[40] V. Ivanyuk, "Forecasting of digital financial crimes in Russia based on machine learning methods," *J. Comput. Virol. Hacking Techn.*, May 2023, doi: 10.1007/s11416-023-00480-3.

[41] M. D. Baknin, D. I. Surzhik, G. S. Vasilyev, and N. V. Dorofeev, "The modeling of the phase-metric method of the geoelectrical control of oil sludge straits," *IOP Conf. Ser., Earth Environ. Sci.*, vol. 459, no. 4, Apr. 2020, Art. no. 042085.

[42] R. Ekhlakov, E. Romanova, E. Dogadina, S. Korchagin, S. Gataullin, J. Mosiej, T. Gataullin, and P. Nikitin, "Modeling the chemical pollution of the area by the random-addition method," *Fractal Fractional*, vol. 6, no. 4, p. 193, Mar. 2022, doi: 10.3390/fractalfract6040193.

[43] O. Kuzichkin, A. Grecheneva, E. Mikhaleva, N. Dorofeev, and B. Maxim, "Application of phase-metric measuring system for geodynamic control of Karst processes," *J. Eng. Appl. Sci.*, vol. 12, no. 4, pp. 6563–6858, 2017.

[44] O. R. Kuzichkin, G. S. Vasilyev, M. D. Baknin, and D. I. Surzhik, "The phase-metric method of isolating the information component in the distributed processing of geoelectric signals in geoecological monitoring systems," *J. Adv. Res. Dyn. Control Syst.*, vol. 12, no. S6, pp. 463–471, 2020.

[45] O. R. Kuzichkin, G. S. Vasilyev, A. V. Grecheneva, E. V. Mikhaleva, M. D. Baknin, and D. I. Surzhik, "Application of phase-metric compensation method for geoelectric control of near-surface geodynamic processes," *Bull. Electr. Eng. Informat.*, vol. 9, no. 3, pp. 898–905, Jun. 2020, doi: 10.11591/eei.v9i3.1727.

[46] O. R. Kuzichkin, R. V. Romanov, N. V. Dorofeev, G. S. Vasilyev, and A. V. Grecheneva, "Hydrogeological monitoring of karst activity based on regime observations in the territory of karst lakes," *J. Water Land Develop.*, no. 48, 2021.

[47] A. Bykov, A. Grecheneva, O. Kuzichkin, D. Surzhik, G. Vasilyev, and Y. Yerbayev, "Mathematical description and laboratory study of electrophysical methods of localization of geodeformational changes during the control of the railway roadbed," *Mathematics*, vol. 9, no. 24, p. 3164, Dec. 2021.

[48] S. Liu, H. Jiang, Z. Wu, and X. Li, "Rolling bearing fault diagnosis using variational autoencoding generative adversarial networks with deep regret analysis," *Measurement*, vol. 168, Jan. 2021, Art. no. 108371, doi: 10.1016/j.measurement.2020.108371.

[49] S. Lee, T. P. Connerton, Y. Lee, D. Kim, D. Kim, and J. Kim, "Semi-GAN: An improved GAN-based missing data imputation method for the semiconductor industry," *IEEE Access*, vol. 10, pp. 72328–72338, 2022, doi: 10.1109/ACCESS.2022.3188871.

[50] X. Wang and H. Liu, "Data supplement for a soft sensor using a new generative model based on a variational autoencoder and Wasserstein GAN," *J. Process Control*, vol. 85, pp. 91–99, Jan. 2020, doi: 10.1016/j.jprocont.2019.11.004.

[51] A. Kositzyn, D. Serdechnyy, S. Korchagin, E. Pleshakova, P. Nikitin, and N. Kurileva, "Mathematical modeling, analysis and evaluation of the complexity of flight paths of groups of unmanned aerial vehicles in aviation and transport systems," *Mathematics*, vol. 9, no. 17, p. 2171, Sep. 2021, doi: 10.3390/math9172171.

[52] Q. Guo, Y. Li, Y. Song, D. Wang, and W. Chen, "Intelligent fault diagnosis method based on full 1-D convolutional generative adversarial network," *IEEE Trans. Ind. Informat.*, vol. 16, no. 3, pp. 2044–2053, Mar. 2020.

[53] X. Liu, D. He, G. Lodewijks, Y. Pang, and J. Mei, "Integrated decision making for predictive maintenance of belt conveyor systems," *Rel. Eng. Syst. Saf.*, vol. 188, pp. 347–351, Aug. 2019.

[54] S. Niu, B. Li, X. Wang, and H. Lin, "Defect image sample generation with GAN for improving defect recognition," *IEEE Trans. Autom. Sci. Eng.*, vol. 17, no. 3, pp. 1611–1622, Jul. 2020.

[55] J. Liu, C. Zhang, and X. Jiang, "Imbalanced fault diagnosis of rolling bearing using improved MsR-GAN and feature enhancement-driven CapsNet," *Mech. Syst. Signal Process.*, vol. 168, Apr. 2022, Art. no. 108664, doi: 10.1016/j.ymssp.2021.108664.

[56] S. Gao, X. Wang, X. Miao, C. Su, and Y. Li, "ASM1D-GAN: An intelligent fault diagnosis method based on assembled 1D convolutional neural network and generative adversarial networks," *J. Signal Process. Syst.*, vol. 91, no. 10, pp. 1237–1247, Oct. 2019, doi: 10.1007/s11265-019-01463-8.

[57] M. Bo, C. Weidong, and Z. Dali, "Intelligent diagnosis method based on GAN sample generation technology," *Vib. Shock*, vol. 39, no. 18, pp. 153–160, 2020.

[58] X. Lin, Z. Xiaotong, and F. Bo, "Fault diagnosis method of motor bearing based on improved GAN algorithm," *J. Northeastern Univ. Natural Sci. Ed.*, vol. 40, no. 12, pp. 1679–1684, 2019.

[59] D. Cabrera, F. Sancho, J. Long, R. Sánchez, S. Zhang, M. Cerrada, and C. Li, "Generative adversarial networks selection approach for extremely imbalanced fault diagnosis of reciprocating machinery," *IEEE Access*, vol. 7, pp. 70643–70653, 2019.

[60] D. Barotov, A. Osipov, S. Korchagin, E. Pleshakova, D. Muzafarov, R. Barotov, and D. Serdechnyy, "Transformation method for solving system of Boolean algebraic equations," *Mathematics*, vol. 9, no. 24, p. 3299, Dec. 2021, doi: 10.3390/math9243299.

[61] S. Sabour, N. Frosst, and G. E. Hinton, "Dynamic routing between capsules," in *Proc. Adv. Neural Inf. Process. Syst.*, vol. 30, 2017, doi: 10.48550/arXiv.1710.09829.

[62] A. V. Vasiliev, A. O. Melnikov, and S. A. Lesko, "Robust neural network filtering in the tasks of building intelligent interfaces," *Russian Technol. J.*, vol. 11, no. 2, pp. 7–19, 2023.

[63] N. Andriyanov, I. Khasanshin, D. Utkin, T. Gataullin, S. Ignar, V. Shumaev, and V. Soloviev, "Intelligent system for estimation of the spatial position of apples based on YOLOv3 and real sense depth camera D415," *Symmetry*, vol. 14, p. 148, 2022, doi: 10.3390/sym14010148.

[64] H. Zhao, Y. Xiao, and Z. Zhang, "Robust semisupervised generative adversarial networks for speech emotion recognition via distribution smoothness," *IEEE Access*, vol. 8, pp. 106889–106900, 2020.

[65] M. T. Pham, J. M. Kim, and C. H. Kim, "Rolling bearing fault diagnosis based on improved GAN and 2-D representation of acoustic emission signals," *IEEE Access*, vol. 10, pp. 78056–78069, 2022.

[66] T. Hahn, M. Pyeon, and G. Kim, "Self-routing capsule networks," in *Proc. Adv. Neural Inf. Process. Syst.*, vol. 32, 2019.

[67] G. E. Hinton, S. Sabour, and N. Frosst, "Matrix capsules with EM routing," in *Proc. Int. Conf. Learn. Represent.*, 2018, doi: 10.13140/RG.2.2.27416.44800.

[68] E. Butun, O. Yildirim, M. Talo, R. S. Tan, and U. R. Acharya, "1D-CADCapsNet: One dimensional deep capsule networks for coronary artery disease detection using ECG signals," *PhysicaMedica*, vol. 70, pp. 39–48, 2020.

[69] R. LaLonde, Z. Xu, I. Irmakci, S. Jain, and U. Bagci, "Capsules for biomedical image segmentation," Dec. 2020, pp. 1–19, *arXiv:2004.04736*.

[70] B. Biswal, P. G. Pavani, T. Prasanna, and P. K. Karn, "Robust segmentation of exudates from retinal surface using M-CapsNet via EM routing," *Biomed. Signal Process. Control*, vol. 68, Jul. 2021, Art. no. 102770.

[71] K. He, X. Zhang, S. Ren, and J. Sun, "Delving deep into rectifiers: Surpassing human-level performance on ImageNet classification," in *Proc. IEEE Int. Conf. Comput. Vis. (ICCV)*. Santiago, Chile: IEEE, Dec. 2015, pp. 1026–1034, doi: 10.48550/arXiv.1502.01852.
[72] A.-R. Lee, Y. Cho, S. Jin, and N. Kim, "Enhancement of surgical hand gesture recognition using a capsule network for a contactless interface in the operating room," *Comput. Methods Programs Biomed.*, vol. 190, Jul. 2020, Art. no. 105385, doi: 10.1016/j.cmpb.2020.105385.
[73] C.-I. Kim, M. Kim, S. Jung, and E. Hwang, "Simplified Fréchet distance for generative adversarial nets," *Sensors*, vol. 20, no. 6, p. 1548, Mar. 2020, doi: 10.3390/s20061548.
[74] A. Fernández, J. A. Sanchidrián, P. Segarra, S. Gómez, E. Li, and R. Navarro, "Rock mass structural recognition from drill monitoring technology in underground mining using discontinuity index and machine learning techniques," *Int. J. Mining Sci. Technol.*, vol. 33, no. 5, pp. 555–571, May 2023, doi: 10.1016/j.ijmst.2023.02.004.
[75] G. Chen, L. Chen, and Q. Li, "Comparison and application of neural networks in LWD lithology identification," *IOP Conf. Ser., Earth Environ. Sci.*, vol. 526, no. 1, Jun. 2020, Art. no. 012146, doi: 10.1088/1755-1315/526/1/012146.
[76] M. L. Arnø, J.-M. Godhavn, and O. M. Aamo, "At-bit estimation of rock density from real-time drilling data using deep learning with online calibration," *J. Petroleum Sci. Eng.*, vol. 206, Nov. 2021, Art. no. 109006, doi: 10.1016/j.petrol.2021.109006.

ALEXEY OSIPOV received the Graduate degree from the Shuisky State Pedagogical Institute, named after D. A. Furmanov, in 1995, with a focus on mathematics and physics, the degree from Moscow State Industrial University, with a focus on applied computer science in economics, in 2007, and the degree from the Ivanovo State University of Chemical Technology, with a focus on labor protection, in 2016. He is currently an employee with the Moscow Technical University of Communications and Informatics, and a candidate of physical and mathematical sciences, in 1999.

EKATERINA PLESHAKOVA graduated from Saratov State Technical University. She is currently an employee with the Moscow Technical University of Communications and Informatics, and a candidate of technical sciences. Her research interests include artificial intelligence and information security.

ARTEM BYKOV was born in Murom, Russia, in 1982. He received the Ph.D. degree, in 2010. In 2010, he defended his dissertation on the design of public address systems. Since 2004, he has been with the Department of Software Engineering, Vladimir State University, Russia. Since 2021, he has been an Associate Professor with the Department of Data Analysis and Machine Learning, Financial University under the Government of the Russian Federation, Russia. He is the author of over 70 articles. His current research interests include data processing and the analysis of geophysical soil control data, and the design of geographic information systems.

OLEG KUZICHKIN received the degree in radio engineering from the Vladimir Polytechnic Institute, in 1984, the Candidate degree in physical and mathematical sciences, and the Doctor of Technical Sciences degree. In 1999, he successfully defended thesis on the topic: "The Monitoring System of Pulsed Geomagnetic Sources" with the Institute of Physics of the Earth, RAS. In 2009, his Doctor of Technical Sciences work: "Theoretical Foundations of Automated Electromagnetic Control of Geodynamic Objects." Currently, he is a Professor with the Department of Information and Robotic Systems, Belgorod State University. His research interests include monitoring and diagnostics systems, radio engineering systems, geodynamic monitoring, measuring equipment, electromagnetic signals, information processing, expert systems, and automated systems.

DMITRY SURZHIK received the degree in radio engineering from Vladimir State University, Russia, in 2012. He defended the thesis of the candidate of technical sciences (Ph.D.) degree in the specialty "Radio engineering, including television systems and devices," in 2017. Since 2017, he has been an Assistant Professor with Vladimir State University. His research interests include geodynamic monitoring, communication networks and systems, signal generation and conversion devices, frequency synthesizers, interference compensation, and approximation methods.

STANISLAV SUVOROV received the master's degree from the Peoples' Friendship University of Russia, with a focus on scientific mathematics, in 1994. Since 1995, he has been a Lecturer with Moscow Industrial University. Since 2005, he has been the Head of the Department of Applied Informatics, the Head of the Bachelor's Degree Program "Big and Open Data," the Head of the Master's Degree Program "System Analytics of Big Data," and the Co-Head of the Professional Retraining Program "Data-Based Management—Chief Data Officer."

SERGEY GATAULLIN received the Graduate degree from the State University of Management. He is currently pursuing the degree in economic sciences. He is a specialist in the mathematical methods of decision-making, economic, and mathematical modeling. He is also the Dean of the Faculty of "Digital Economy and Mass Communications," Moscow Technical University of Communications and Informatics.